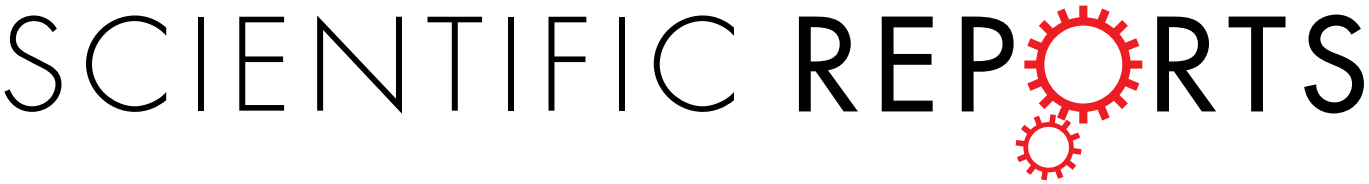

OPEN

Ti^{3+}-self doped brookite TiO_2 single-crystalline nanosheets with high solar absorption and excellent photocatalytic CO_2 reduction

Received: 08 January 2016
Accepted: 08 March 2016
Published: 29 March 2016

Xiaoye Xin[1], Tao Xu[2], Lan Wang[1] & Chuanyi Wang[1]

Black brookite TiO_2 single-crystalline nanosheets with outstanding photocatalytic activity toward CO_2 reduction is prepared by a facile oxidation-based hydrothermal reaction method combined with post-annealing treatment. Large amount of Ti^{3+} defects are introduced into the bulk of brookite nanoparticles, which increases the solar energy absorption and enhances the photocatalytic activity.

The emission of greenhouse gases, particularly carbon dioxide (CO_2), could result in the global climate change and unhealthful regional air quality[1,2]. To reduce the emission of CO_2 and to achieve a sustainable energy future, novel materials and new promising "green chemistry" technologies are desired to convert CO_2 into useful chemical compounds and fuels using sunlight. CO_2 photoreduction in engineered systems, however, still faces severe challenges like low conversion yields and quantum efficiencies due to fast electron-hole recombination, narrow sunlight absorption range, and backward reactions[3–6]. Strategies to resolve those challenges have been a research hotspot in the area[7–10]. Among the studied semiconductor photocatalysts, titanium dioxide (TiO_2) is by far the most popular catalyst because of its low cost, suitable bandgap and nature abundance[11–13]. From this prospect, TiO_2 is still a promising photocatalyst for CO_2 photoreduction due to its favorable band edges because TiO_2 has a higher CB edge, which will promote the reaction of CO_2 reduction with H_2O that has a high reduction potential[14].

TiO_2 naturally exists in three polymorphs: anatase, brookite and rutile. Among them, only TiO_2 anatase, rutile, and anatase-rutile mixed phase (e.g., Degussa P25) have been studied for CO_2 photoreduction[15]. In other words, naturally occurring metastable brookite is the least investigated one because of the difficulties to obtain its pure form[16]. Based on the previous model for the structure-property relationship of photo-catalytic materials, the photocatalytic activity of brookite would be inferior to anatase but superior to rutile[17–19]. For brookite, lower packing factor, in accordance with higher structural openness degree, is associated with stronger ability for electron-hole separation and transfer, and usually results in better photocatalytic activity[20,21]. Considering that brookite has a relative open structure, its photocatalytic performance is worth investigating such as in CO_2 photoreduction.

Many efforts have been made in decades to improve the photocatalytic activity of brookite, including preparation of nanosized brookite with various morphologies and studies of the involved shape-dependent photocatalytic performance[22–26]. However, the application of brookite TiO_2 has been limited to the ultraviolet (UV) range, which makes it an inefficient photocatalyst for fully exploiting solar light. Narrowing down the TiO_2 bandgap to turn it into an efficient material for solar energy conversion has been an ongoing challenge. Recently, the chemistry of structurally defective TiO_2 with Ti^{3+} self-doping has been developed to solve the challenges in broad spectral range of photon absorption. Reduction of Ti^{4+} into Ti^{3+} is often achieved by harsh and costly physical methods, such as high temperature and pressurized hydrogenation[27–30], plasma treatment[31,32], vacuum activation and electron beams irradiation[33] to improved light absorption and photocatalytic activities. Thus, a facile method is greatly desired to get defective brookite TiO_2 with Ti^{3+} self-doping.

In this work, we developed an innovative facial oxidation-based hydrothermal method to synthesize bulk Ti^{3+} self-doped brookite TiO_2 single-crystalline nanosheets (denoted as TiO_{2-x} if no further heat treatment). By post-annealing at different temperatures, Ti^{3+} self-doped brookite TiO_2 with controllable amounts of Ti^{3+} defects

[1]Laboratory of Environmental Sciences and Technology, Xinjiang Technical Institute of Physics & Chemistry; Key Laboratory of Functional Materials and Devices for Special Environments, Chinese Academy of Sciences, Urumqi 830011, China. [2]Department of Chemistry and Biochemistry, Northern Illinois University, DeKalb, IL 60115, USA. Correspondence and requests for materials should be addressed to L.W. (email: wanglan@ms.xjb.ac.cn) or C.W. (email: cywang@ms.xjb.ac.cn)

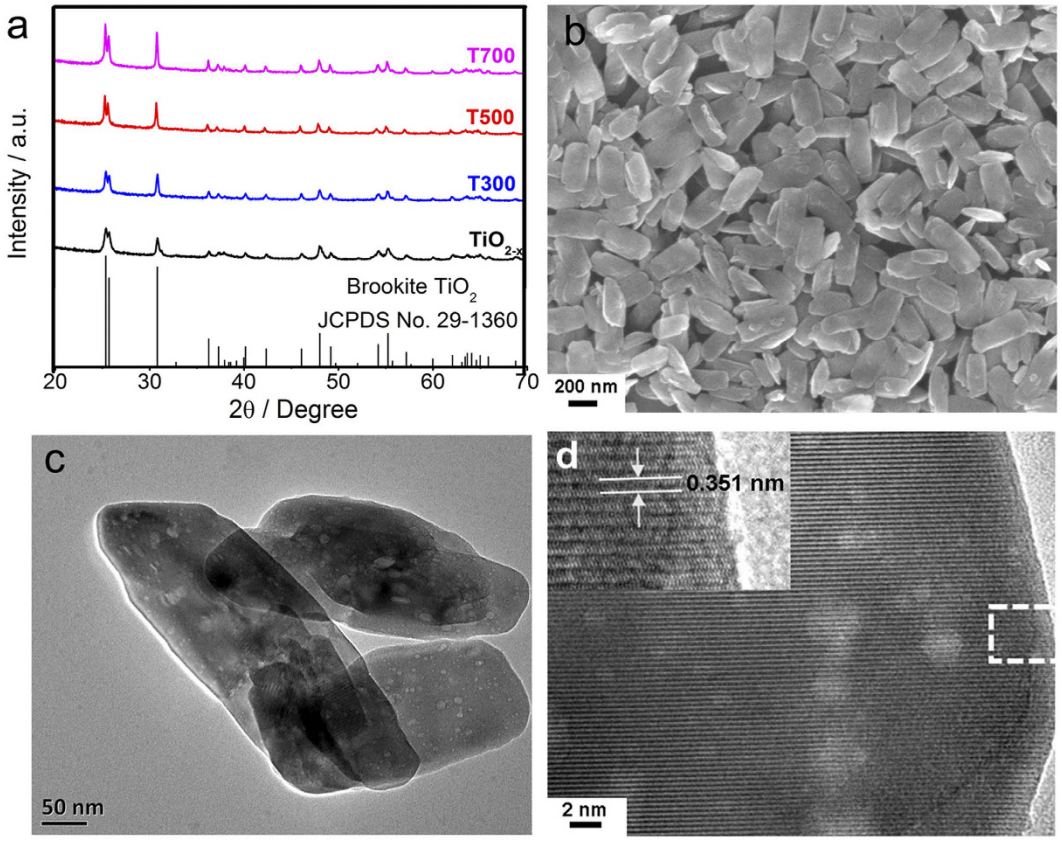

Figure 1. (**a**) XRD patterns of as-prepared brookite TiO_{2-x} and the blue TiO_{2-x} after postannealing treatment at different temperatures for 3 h. (**b**) SEM image of the typical T500 sample. (**c**) TEM image of the T500 sample. (**d**) HRTEM image taken from the edge of the single crystal.

is achieved. The black brookite TiO_{2-x} (T500) shows drastically enhanced visible-light absorption and exhibits excellent photocatalytic activity toward CO_2 reduction.

Results

The X-ray diffraction (XRD) patterns of the high quality brookite Ti^{3+}-self doped TiO_2 is displayed in Fig. 1a. The patterns show that all the samples are pure brookite phase without any other impurity phase (rutile or anatase phase). All the diffraction positions and intensity distributions can be indexed to the brookite corresponding to the JCPDS card No. 29–1360. By increasing the post-annealing temperature, the characteristic diffraction peaks of defective brookite TiO_2 becomes stronger and sharper due to the increase in the crystallinity. When the temperature reaches 700 °C, no rutile or anatase characteristic diffraction peaks were detected, indicating that the brookite phase can be stabilized at higher temperatures.

The morphology of the synthesized brookite powders is investigated by scanning electron microscopy (SEM) and transmission electron microscopy (TEM) as shown in Fig. 1b,c, respectively. Clearly, the Ti^{3+}-self doped brookite shows platelike features with uniform sizes of length up to 400 nm and thickness up to 10 nm. The obtained TiO_2 particles are uniformly dispersed without obvious aggregation. There is no further particle growth with an increase of the post-annealing temperature. Distinct crystal planes and smooth fringes can be observed clearly from the magnified image of a single particle as shown in Fig. 1c.

In order to unveil the microstructure transformation of the brookite after post-annealing treatment, the TiO_{2-x} sample treated at 500 °C were examined by high resolution transmission electron microscopy (HRTEM) as shown in Fig. 1d. The uniform lattices indicate that the Ti^{3+} self-doped brookite TiO_2 nanoparticles are highly crystallized. In addition, the spacing of the fringes paralleling to the top and bottom of the vertical nanoplate is 0.351 nm (Fig. 1d, inset), which can be attributed to the (210) facet of brookite. There is no obvious difference in lattice fringes width (e.g., those for rutile phase or TiH_2) indicating that the as-prepared sample is pure brookite phase. This result is consistent with XRD analysis. Additionally, as shown in Fig. 2, there is no obvious difference among the other samples, indicating that the temperature change has very limited influence on the morphology and crystallite size of these nanocrystals.

The top insert of Fig. 3 is photographic images of Ti^{3+} self-doped brookite TiO_2 samples prepared with postannealing treatment at different temperatures for 3 h in a N_2 gas flow and their optical band gap estimated by Kubelka-Munk function. The results show that the color of brookite TiO_2 samples is remarkably different from white perfect TiO_2 nanocrystal particles. From previous research, this phenomenon indicates the existence of Ti^{3+} defects[30]. The color of the brookite turns from blue to brown (T300) and further to black (T500). The color

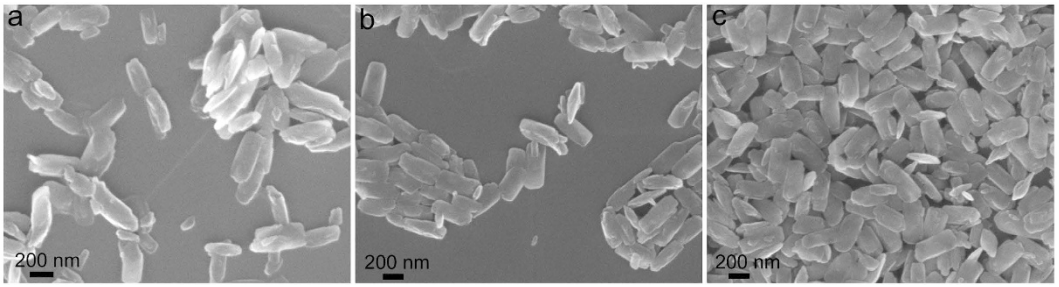

Figure 2. SEM images of (**a**) TiO_{2-x}, (**b**) T300, and (**c**) T700.

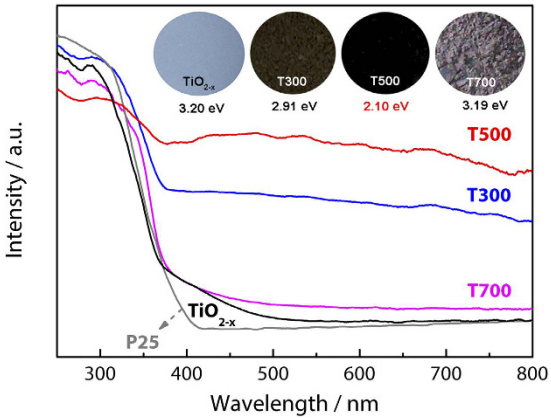

Figure 3. UV-vis diffuse reflectance spectra of the as-prepared brookite TiO_{2-x}, T300, T500 and T700.

variation indicates the enhanced light absorption of brookite after post-annealing treatment up to 500 °C. As the post-annealing treatment temperature further increases, the dark black color is not maintained but gradually faded to a light grey blue at 700 °C.

Figure 3 displays the UV-vis diffuse reflectance spectra (UV-vis DRS) of as-prepared brookite TiO_{2-x}, T300, T500 and T700 nanoparticles, and Deguass P25 as reference was also examined. The absorption peak at 390 nm is attributed to the intrinsic bandgap absorption of crystalline brookite TiO_{2-x}. The as-prepared TiO_{2-x} sample (blue in color) exhibits an obvious stronger absorption between 400 and 800 nm compared to P25. This strong absorption is attributed to the existence of Ti^{3+} defects which induce a continuous vacancy band of electronic states just below the conduction band edge of TiO_{2-x}. The existence of Ti^{3+} defects is supported by ESR measurements that will be discussed in later section. Compared with TiO_{2-x}, the absorption in the visible light region is greatly enhanced after post-annealing treatment. As the annealing temperature increases from 300 °C to 500 °C, the light absorption increases gradually, in good agreement with the color transformation of brookite. However, the light absorption of T700 presents a dramatically decrease in comparison with the T500 sample, which is coincident with the observed color change trend of the samples (as depicted in the insert of Fig. 3). In the hydrothermally treated brookiteTiO_{2-x}, the enhanced visible-light absorption is attributed to the fact that hydrothermally treated process introduces the disorder in the TiO_2 and the resulted bandgap narrowing[34], For the black brookite TiO_2, postannealing treatment not only increases the structural openness, but also introduces Ti^{3+} ($3d^1$) in the TiO_{2-x} bulk[35], Using the Kubelka–Munk function as the vertical axis to plot it against the photon energy, the optical band gaps of all samples can be derived, and the results are summarized in the top insert of Fig. 3. Among all the samples, the band gap of T500 (2.10 eV) is the narrowest one. These aspects may work together leading to the black colouration, enhanced light absorption and promoted photocatalytic activity of defective brookite TiO_2.

In this work, photoactivity of as prepared defective brookite TiO_{2-x} was explored by the heterogeneous photoreduction of CO_2 under visible light illumination (Fig. 4). CH_4 and CO were detected as the major hydrocarbon products from the photoreduction of CO_2 over the as-synthesized Ti^{3+}-self doped brookite TiO_2 photocatalysts. The yields of CH_4 and CO ($\mu mol/g_{cat}$) attained after 6 h of visible-light irradiation are shown in Fig. 4a,b (detailed calculation can refer to Eq. 1).

$$\text{Total } CH_4/CO \text{ yield} = \frac{\text{total amount of } CH_4/CO \text{ produced } (\mu\text{mol})}{\text{amount of photocatalyst used (g-catalyst)}} \quad (1)$$

Discussion

The low symmetry and large unit cell of brookite result in a diagnostically complex Raman spectrum compared to the other two polymorphs (anatase and rutile), thus Raman spectroscopy has been widely used to detect the

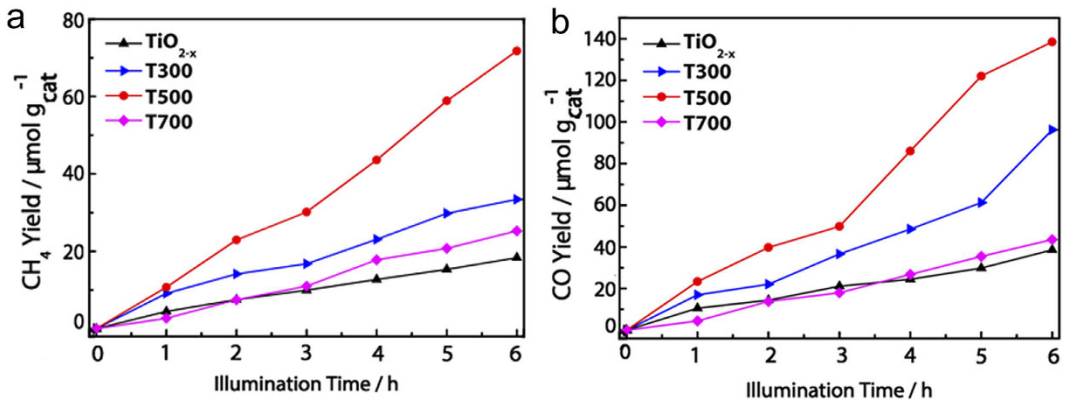

Figure 4. (**a**) CH_4 and (**b**) CO evolution over the brookite TiO_{2-x}, T300, T500 and T700 samples for a period of 6 h visible-light illumination ($\lambda \geq 420$ nm).

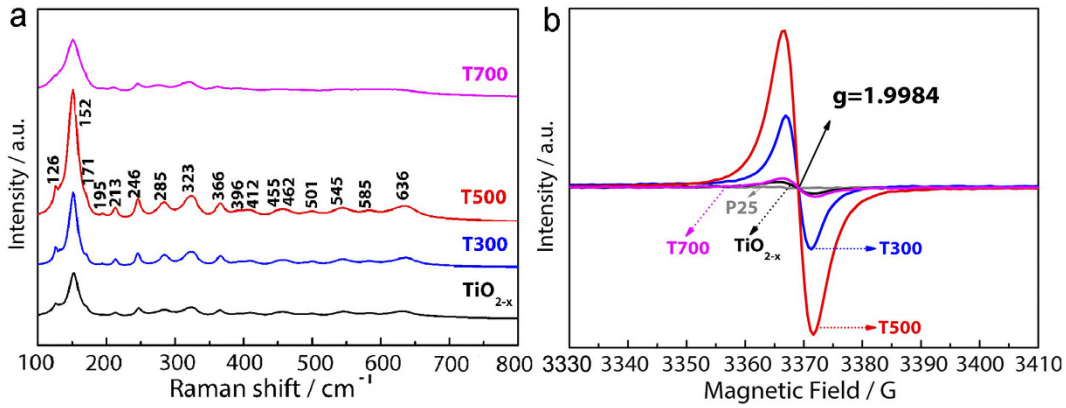

Figure 5. (**a**) Raman spectra and (**b**) low-temperature EPR spectra of the brookite TiO_{2-x}, T300, T500 and T700 samples.

presence of the brookite phase in TiO_2 containing materials[25]. Therefore, Raman spectra of the before and after post-annealing treatment can further confirm the phase composition. As shown in Fig. 5a, the TiO_{2-x} and the annealed defective TiO_2 at different temperatures display the typical Raman spectra of brookite, and 16 bands are identified in total, including seven A_{1g} (124, 151, 192, 244, 410, 544, 636 cm^{-1}), four B_{1g} (211, 318, 415, 500 cm^{-1}), four B_{2g} (365, 393, 460, 581 cm^{-1}), and one B_{3g} (287 cm^{-1}). The characteristic Raman signals at 399 cm^{-1} and 519 cm^{-1} for anatase or at 447 cm^{-1} and 612 cm^{-1} for rutile are not observed. This further proves the high phase purity of brookite for the TiO_{2-x} and the annealed defective TiO_2 samples, in good agreement with the XRD results.

In addition, the intensity of high-resolution Eg Raman vibration modes increases as the post-annealing treatment temperature increases up to 500 °C. This is attributed to the effect of enhanced crystallinity upon the increase in annealing temperature, because higher crystallinity contains more Raman active facets, which is proportional to the Eg intensity fluctuations. When the temperature increases to 700 °C, the intensity of Raman vibration modes is decreased and the peak width is broadened, which may be due to the change in the distribution and concentration of Ti^{3+}. The fact that the Ti^{3+}-doped TiO_2 has quite different high-resolution Eg modes in Raman spectra with different defects distribution and concentration suggests that Ti^{3+} should mainly localize within the bulk of the samples.

Electron paramagnetic resonance (EPR), which is highly sensitive to paramagnetic species containing unpaired electrons, has been widely used to characterize the existence of Ti^{3+} defects. As indicated in Fig. 5b, the pristine TiO_2 contains almost completely Ti^{4+} ($3d^0$) and shows a negligible paramagnetic signal peak under the present EPR measurement condition at 110 K. In general, the surface Ti^{3+} tends to adsorb O_2, which could be reduced to superoxide radical anions (O^{2-}) with an EPR signal feature at $g = 2.02$[36]. However, no such signal appears for all samples, further demonstrating the absence of surface Ti^{3+}.

On the other hand, the EPR spectra of brookite defective TiO_2 nanoparticles show intense axially symmetry signals centered at the g value of 1.9984, which have been reported for Ti^{3+} ions in brookite crystallite[37], indicating that the free electrons occupy interior Ti position thereby generating Ti^{3+} defects in bulk. Accordingly, the chemical equation in our work can be expressed as below:

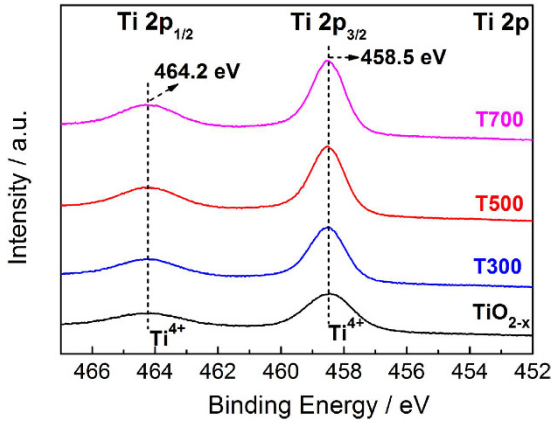

Figure 6. Ti 2p XPS spectra of the brookite TiO_{2-x}, T300, T500 and T700 samples.

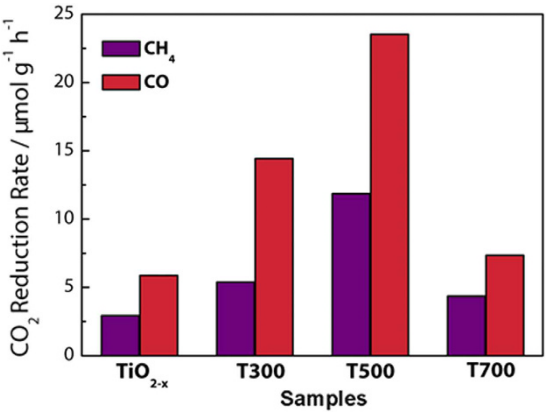

Figure 7. CO_2 reduction rate of the brookite TiO_{2-x}, T300, T500 and T700 samples.

$$Ti^{2+} + H_2O_2 + OH^- + BH_4^- \rightarrow Ti^{3+} + Ti^{4+} + BO_2^- + H_2O + H_2\uparrow \quad (2)$$

Furthermore, the EPR intensity increases along with the post-annealing temperature. The strongest value is obtained for T500, but the signal intensity declines sharply when further increasing the treatment temperature to 700 °C. By numerical double integration of the EPR spectra with an aqueous solution of Cu^{2+} as reference, the amount of Ti^{3+} centers for TiO_{2-x} sample is calculated to be 0.7×10^{19} spins/mol, equivalent to one Ti^{3+} out of every 2.9×10^4 Ti^{4+}. Whereas, the amount of Ti^{3+} centers for T500 sample is almost 10 times larger than that for TiO_{2-x}, namely, one Ti^{3+} in every 2.9×10^3 Ti^{4+}. This suggests that the concentration of bulk Ti^{3+} defect is greatly enhanced by the high temperature post-annealing treatment. From our previous study, the decreased Ti^{3+} defects upon treatment at 700 °C is mainly due to the difficulty of further diffusion of Ti^{3+} in enhanced crystallinity, leading to the dilution of the "colour center"[38].

In order to confirm the existence of Ti^{3+}, additional characterizations are performed. X-ray photoelectron spectroscopy (XPS) is performed to further investigate the transformation of surface chemical bonding and to detect the electronic valence band position of the brookite samples. As shown in Fig. 6, the Ti 2p XPS spectra of brookite TiO_{2-x}, T300, T500 and T700 samples show the typical pattern of Ti^{4+} –O bonds in TiO_2 with Ti $2p_{3/2}$ and $2p_{1/2}$ peaks centered at binding energies of 458.5 eV and 464.2 eV[39]. For all the samples, no peaks shift apparently to lower energy, indicating that Ti^{3+} species are separately located at bulk of the samples, and no different chemical states and disorders on the surface of samples. This agrees with the HRTEM observation, i.e., no obvious disordered layer in the edge of the samples.

The CO_2 reduction rate is presented in Fig. 7. The CO_2 reduction rate of annealed brookite TiO_2 also improves dramatically; it shows drastically enhanced CO_2 reduction rate when brookite TiO_{2-x} is annealled at 500 °C (11.9 $\mu mol \cdot g_{cat}^{-1} h^{-1}$ for CH_4 and 23.5 $\mu mol \cdot g_{cat}^{-1} h^{-1}$ for CO). However, defective brookite prepared at 700 °C shows lower CO_2 reduction rate (4.4 $\mu mol \cdot g_{cat}^{-1} h^{-1}$ for CH_4 and 7.3 $\mu mol \cdot g_{cat}^{-1} h^{-1}$ for CO), but is still higher than untreated TiO_{2-x} sample. It can be deduced that the photocatalytic reduction performance agrees well with the light absorption and Ti^{3+} defects (numbers and distribution); the more the light absorption and the Ti^{3+} defects, the higher the photocatalytic reduction activity is.

Clearly, the engineered Ti^{3+}-self doped brookite catalysts developed in this work demonstrate a superior activity. It is the first time to present a facile approach to controllablly synthesize Ti^{3+}-self doped brookite TiO_2 as an

outstanding candidate for CO_2 photoreduction to produce CO and CH_4. Further study on the selectivity of CO_2 reduction is going on.

In summary, this work illustrates that the oxidation-based hydrothermal synthesis of Ti^{3+} self-doped brookite TiO_2 is an effective strategy to prepare uniform Ti^{3+} self-doped brookite TiO_2 nanosheets. The introduction of Ti^{3+} defects in the bulk of brookite enhances the visible light absorption and narrows the bandgap. Our study demonstrates that brookite can be successfully tuned to be highly active toward photocatalytic performance for CO_2 reduction through post-annealing at different temperatures, which illuminates the future research of brookite; the oxidation-based hydrothermal synthesis combined with post-annealing treatment may provide a novel path for tuning the photocatalysts from relatively inert to highly active and shine light on the greenhouse gases conversion into sustainable energy.

Methods

Materials. Titanium hydride (TiH_2, 98.0%) powder was purchased from Sigma–Aldrich Co., LLC. Hydrogen peroxide (H_2O_2, 30.0%), sodium borohydride ($NaBH_4$, 98.0%), hydrochloric acid (HCl, 36–38%, A.R.) and sodium hydroxide (NaOH, 98%, A.R.) were obtained from Sinopharm Chemical Reagent Co., Ltd. and used as received without any further purification. Double distilled water was used throughout the experiments.

Synthesis of Ti^{3+} self-doped brookite TiO_2 nanoparticles. In a typical synthetic process, TiH_2 (0.256 g) and H_2O (2 mL) were mixed in a 50 mL round-bottomed flask magnetically stirred for 5 min. Then H_2O_2 (30 mL 30.0 wt%) as the oxidation was added dropwise to this dark gray suspensions, and this mixture was vigorously stirred for 12 h till it changed to yellowish gel-like state. After that, double distilled water (40 mL) was added under continuous magnetic stirring. A certain amount of NaOH (1.0 M) solution as the pH regulator was added gradually until the pH of the mixture solution was tuned to 9.0. $NaBH_4$ (0.4 g) as reducing agent was added to this light yellow transparency mixture and then transferred to the Teflon-lined stainless-steel autoclave immediately and hydrothermally treated at 180 °C for 24 h. The sample was then collected and added into HCl (50.0 mL, 1.0 M) solution to eliminate the sodium boron compounds. After stirring for 10 h, the powders were washed by distilled water and ethanol repetitively to remove the impurities (e.g., Na^+, Cl^-, BO_3^{2-}). The obtained precipitate was dried under vacuum for 12 h to yield a grey blue TiO_2 nanocrystals powder, denoted as TiO_{2-x}. Postannealing treatment of the TiO_{2-x} sample was conducted under a N_2 gas flow (150 sccm) in a tube furnace at an elevated temperature of 300 °C, 500 °C and 700 °C for 3 h. Therefore, the samples obtained at the specific temperatures are designated as T300, T500 and T700, respectively.

Characterization. The crystal structures of the samples were identified on a Bruker D8 X-ray diffractometer with Cu Kα radiation ($\lambda = 0.15418$ nm). The morphology photographs of the samples were recorded by field emission scanning electron microscopy (FESEM; ZEISS SUPRA55VP) and transmission electron microscopy (TEM, JEOL-JEM 2100). Ultraviolet–visible (UV–vis) diffusion reflectance spectra of the samples were obtained on a SolidSpec-3700DUV spectrophotometer (Shimadzu) using $BaSO_4$ as reference to obtain absorption spectra for determining the band gap. Raman spectra were obtained on a laser Raman spectrometer (LabRAM HR Evolution RAMAN SPECTROMETER, HORIBA Scientific Ltd.) with a back scattering configuration using an Ar^+ laser (20 mW, 532 nm) as excitation source. The surface electronic state analysis was studied by X-ray photoelectron spectra (XPS), and the measurements were carried out on an X-ray photoelectron spectrometer (ESCALAB MK II) using Mg Ka (1253.6 eV) X-rays as the excitation source, with C 1s (284.6 eV) for calibration. Electron paramagnetic resonance (EPR) spectra were recorded on a Bruker Elexsys E500 spectrometer by applying an X-band (9.43 GHz, 1.5 mW) microwave with sweeping magnetic field at 110 K in cells that can be connected to a conventional high-vacuum apparatus (residual pressure $< 10^{-4}$ mbar). The concentration of Ti^{3+} was determined by a numerical double integration of the EPR spectra in comparison with an aqueous solution of Cu^{2+}.

Photocatalitic reduction of CO_2 under visible-light. The photocatalytic activities of the Ti^{3+}-self doped brookite TiO_2 single-crystalline nanosheets were studied using a CO_2 photoreduction system at ambient condition in a continuous gas flow reactor. The CO_2 photoreduction process was performed under visible light irradiation with a 300 W Xe lamp (PLS-SXE300, Perfect Light Company, Beijing, China) equipped with an ultraviolet cut-off filter to provide visible light ($\geq$420 nm). The illumination intensity at the surface was 0.216 W/cm^2 as measured by a calibrated precision optical power meter (1916-C, Newport Corp.). The amount of photocatalyst used was held constant in all runs. Highly pure CO_2 (99.99%) was bubbled through water to produce a mixture of CO_2 and water vapor into the photoreactor at atmospheric pressure. Before switching on the light source, wet CO_2 was permitted to flow through the photoreactor at 30 mL/min for 30 min to eliminate any excess air and to ensure the complete adsorption of gas molecules. The photoreactor was operated in a continuous flow mode (2.0 mL/min flow rate), and the gaseous products in the reactor effluent were continuously analyzed for 6 h by a gas chromatograph (GC, Agilent 7890 A) equipped with both a thermal conductivity detector (TCD) and a flame ionization detector (FID).

References

1. An, C. H. *et al.* Strongly visible-light responsive plasmonic shaped AgX:Ag (X = Cl, Br) nanoparticles for reduction of CO_2 to methanol. *Nanoscale* **4,** 5646 (2012).
2. Anpo, M., Yamashita, H., Ichihashi, Y. & Ehara, S. Photocatalytic reduction of CO_2 with H_2O on various titanium-oxide catalysts. *J. Electroanal. Chem.* **396,** 21 (1995).
3. Usubharatana, P., McMartin, D., Veawab, A. & Tontiwachwuthikul, P. Photocatalytic process for CO_2 emission reduction from industrial flue gas streams. *Ind. Eng. Chem. Res.* **45,** 2558 (2006).
4. Indrakanti, V. P., Kubicki, J. D. & Schobert, H. H. Photoinduced activation of CO_2 on Ti-based heterogeneous catalysts: Current state, chemical physics-based insights and outlook. *Energ. Environ. Sci.* **2,** 745 (2009).

5. Fujishima, A., Zhang, X. T. & Tryk, D. A. TiO_2 photocatalysis and related surface phenomena. *Surf. Sci. Rep.* **63,** 515 (2008).
6. Linsebigler, A. L., Lu, G. Q. & Yates, J. T. Photocatalysis on TiO_2 Surfaces-principles, mechanisms, and selected results. *Chem. Rev.* **95,** 735 (1995).
7. Sim, L. C., Leong, K. H., Saravanan, P. & Ibrahim, S. Rapid thermal reduced graphene oxide/Pt-TiO_2 nanotube arrays for enhanced visible-light-driven photocatalytic reduction of CO_2. *Appl. Surf .Sci.* **358,** 122 (2015).
8. Yuan, L. & Xu, Y. J. Photocatalytic conversion of CO_2 into value-added and renewable fuels. *Appl. Surf. Sci.* **342,** 154 (2015).
9. Li, Y. F. *et al.* Octahedral Cu_2O-modified TiO_2 nanotube arrays for efficient photocatalytic reduction of CO_2. *Chinese J. Catal.* **36,** 2229 (2015).
10. Akple, M. S. *et al.* Nitrogen-doped TiO_2 microsheets with enhanced visible light photocatalytic activity for CO_2 reduction. *Chinese J. Catal.* **36,** 2127 (2015).
11. Ganesh, V. A., Raut, H. K., Nair, A. S. & Ramakrishna, S. A review on self-cleaning coatings. *J. Mater. Chem.* **21,** 16304 (2011).
12. Wu, D. Y. & Long, M. C. Realizing visible-light-induced self-cleaning property of cotton through coating N-TiO_2 film and loading AgI particles. *Acs. Appl. Mater. Inter.* **3,** 4770 (2011).
13. Yaghoubi, H., Taghavinia, N., Alamdari, E. K. & Volinsky, A. A. Nanomechanical properties of TiO_2 granular thin films. *Acs. Appl. Mater. Inter.* **2,** 2629 (2010).
14. Nowotny, J., Bak, T., Nowotny, M. K. & Sheppard, L. R. TiO_2 surface active sites for water splitting. *J. Phys. Chem. B* **110,** 18492 (2006).
15. Di Paola, A., Bellardita, M. & Palmisano, L. Brookite, the least known TiO_2 photocatalyst. *Catalysts* **3,** 36 (2013).
16. Iskandar, F. *et al.* Enhanced photocatalytic performance of brookite TiO_2 macroporous particles prepared by spray drying with colloidal templating. *Adv. Mater.* **19,** 1408 (2007).
17. Liu, L. J. & Li, Y. Understanding the reaction mechanism of photocatalytic reduction of CO_2 with H_2O on TiO_2-based photocatalysts: a review. *Aerosol. Air Qual. Res.* **14,** 453 (2014).
18. Kumar, S. G. & Rao, K. S. R. K. Polymorphic phase transition among the titania crystal structures using a solution-based approach: from precursor chemistry to nucleation process. *Nanoscale* **6,** 11574 (2014).
19. Cargnello, M., Gordon, T. R. & Murray, C. B. Solution-phase synthesis of titanium dioxide nanoparticles and nanocrystals. *Chem. Rev.* **114,** 9319 (2014).
20. Kandiel, T. A., Feldhoff, A., Robben, L., Dillert, R. & Bahnemann, D. W. Tailored titanium dioxide nanomaterials: anatase nanoparticles and brookite nanorods as highly active photocatalysts. *Chem. Mater.* **22,** 2050 (2010).
21. Pottier, A., Chaneac, C., Tronc, E., Mazerolles, L. & Jolivet, J. P. Synthesis of brookite TiO_2 nanoparticles by thermolysis of $TiCl_4$ in strongly acidic aqueous media. *J. Mater. Chem.* **11,** 1116 (2001).
22. Xu, J. L., Li, K., Shi, W. Y., Li, R. J. & Peng, T. Y. Rice-like brookite titania as an efficient scattering layer for nanosized anatase titania film-based dye-sensitized solar cells. *J. Power Sources* **260,** 233 (2014).
23. Zhao, B., Chen, F., Huang, Q. W. & Zhang, J. L. Brookite TiO_2 nanoflowers. *Chem. Commun*. **5115** (2009).
24. Hall, S. R., Swinerd, V. M., Newby, F. N., Collins, A. M. & Mann, S. Fabrication of porous titania (brookite) microparticles with complex morphology by sol-gel replication of pollen grains. *Chem. Mater.* **18,** 598 (2006).
25. Lin, H. F. *et al.* Synthesis of high-quality brookite TiO_2 single-crystalline nanosheets with specific facets exposed: tuning catalysts from inert to highly reactive. *J. Am. Chem. Soc.* **134,** 8328 (2012).
26. Deng, Q. X. *et al.* Brookite-type TiO_2 nanotubes. *Chem. Commun*. **3657** (2008).
27. Liu, H. *et al.* The enhancement of TiO_2 photocatalytic activity by hydrogen thermal treatment. *Chemosphere* **50,** 39 (2003).
28. Shin, J. Y., Joo, J. H., Samuelis, D. & Maier, J. Oxygen-deficient TiO_2-delta nanoparticles via hydrogen reduction for high rate capability lithium batteries. *Chem. Mater.* **24,** 543 (2012).
29. Naldoni, A. *et al.* Effect of nature and location of defects on bandgap narrowing in black TiO_2 nanoparticles. *J. Am. Chem. Soc.* **134,** 7600 (2012).
30. Wang, G. M. *et al.* Hydrogen-treated TiO_2 nanowire arrays for photoelectrochemical water splitting. *Nano. Lett.* **11,** 3026 (2011).
31. Nakamura, I., Sugihara, S. & Takeuchi, K. Mechanism for NO photooxidation over the oxygen-deficient TiO_2 powder under visible light irradiation. *Chem. Lett*. **1276** (2000).
32. Zhang, Z. K., Bai, M. L., Guo, D. Z., Hou, S. M. & Zhang, G. M. Plasma-electrolysis synthesis of TiO_2 nano/microspheres with optical absorption extended into the infra-red region. *Chem. Commun.* **47,** 8439 (2011).
33. Xing, M. Y., Zhang, J. L., Chen, F. & Tian, B. Z. An economic method to prepare vacuum activated photocatalysts with high photo-activities and photosensitivities. *Chem. Commun.* **47,** 4947 (2011).
34. Chen, X. B., Liu, L., Yu, P. Y. & Mao, S. S. Increasing solar absorption for photocatalysis with black hydrogenated titanium dioxide nanocrystals. *Science* **331,** 746 (2011).
35. Zhu, G. L. *et al.* Black brookite titania with high solar absorption and excellent photocatalytic performance. *J. Mater. Chem. A* **1,** 9650 (2013).
36. Anpo, M. *et al.* Generation of superoxide ions at oxide surfaces. *Top Catal*. **8,** 189 (1999).
37. Livraghi, S. *et al.* Nature of reduced states in titanium dioxide as monitored by electron paramagnetic resonance. II: rutile and brookite cases. *J. Phys. Chem. C* **118,** 22141 (2014).
38. Xin, X. Y., Xu, T., Yin, J., Wang, L. & Wang, C. Y. Management on the location and concentration of Ti^{3+} in anatase TiO_2 for defects-induced visible-light photocatalysis. *Appl .Catal .B:Environ*. **176,** 354 (2015).
39. Xiong, L. B., Li, J. L., Yang, B. & Yu, Y. Ti^{3+} in the surface of titanium dioxide: generation, properties and photocatalytic application. *J. Nanomater.* **831524** (2012).

Acknowledgements

Financial support by the National Nature Science Foundation of China (Grant Nos 21473248, 21428305, 21303258), the Xinjiang International Science & Technology Cooperation Program, China (20146006), the Western Light Program of Chinese Academy of Sciences (XBBS201211), the CAS/SAFEA International Partnership Program for Creative Research Teams, the Natural Science Foundation of Xinjiang (2013211B33), the Xinjiang Program of Cultivation of Young Innovative Technical Talents (2013731019), and the "Western Action Plan" (KGZD-EW-502) is gratefully acknowledged. TX acknowledges the support from the U.S National Science Foundation (CBET 1150617).

Author Contributions

X.X. and L.W. performed the experiments and wrote the main manuscript text. C.W. guided the whole work. T.X. made contribution for discussions and critical revision of the manuscript. All authors reviewed the manuscript.

Additional Information

Competing financial interests: The authors declare no competing financial interests.

How to cite this article: Xin, X. *et al.* Ti^{3+}-self doped brookite TiO_2 single-crystalline nanosheets with high solar absorption and excellent photocatalytic CO_2 reduction. *Sci. Rep.* **6**, 23684; doi: 10.1038/srep23684 (2016).

This work is licensed under a Creative Commons Attribution 4.0 International License. The images or other third party material in this article are included in the article's Creative Commons license, unless indicated otherwise in the credit line; if the material is not included under the Creative Commons license, users will need to obtain permission from the license holder to reproduce the material. To view a copy of this license, visit http://creativecommons.org/licenses/by/4.0/